Environmental Science & Technology

Article

pubs.acs.org/est

In Situ Measurement of Magnesium Carbonate Formation from CO_2 Using Static High-Pressure and -Temperature ^{13}C NMR

J. Andrew Surface,[†] Philip Skemer,[‡] Sophia E. Hayes,*[,†] and Mark S. Conradi*[,§]

[†]Department of Chemistry, Washington University, 1 Brookings Drive, St. Louis, Missouri 63130, United States

[‡]Department of Earth and Planetary Sciences, Washington University, 1 Brookings Drive, St. Louis, Missouri 63130, United States

[§]Department of Physics, Washington University, 1 Brookings Drive, St. Louis, Missouri 63130, United States

Supporting Information

ABSTRACT: We explore a new in situ NMR spectroscopy method that possesses the ability to monitor the chemical evolution of supercritical CO_2 in relevant conditions for geological CO_2 sequestration. As a model, we use the fast reaction of the mineral brucite, $Mg(OH)_2$, with supercritical CO_2 (88 bar) in aqueous conditions at 80 °C. The in situ conversion of CO_2 into metastable and stable carbonates is observed throughout the reaction. After more than 58 h of reaction, the sample was depressurized and analyzed using in situ Raman spectroscopy, where the laser was focused on the undisturbed products through the glass reaction tube. Postreaction, ex situ analysis was performed on the extracted and dried products using Raman spectroscopy, powder X-ray diffraction, and magic-angle spinning ^1H-decoupled ^{13}C NMR. These separate methods of analysis confirmed a spatial dependence of products, possibly caused by a gradient of reactant availability, pH, and/or a reaction mechanism that involves first forming hydroxy-hydrated (basic, hydrated) carbonates that convert to the end-product, anhydrous magnesite. This carbonation reaction illustrates the importance of static (unmixed) reaction systems at sequestration-like conditions.

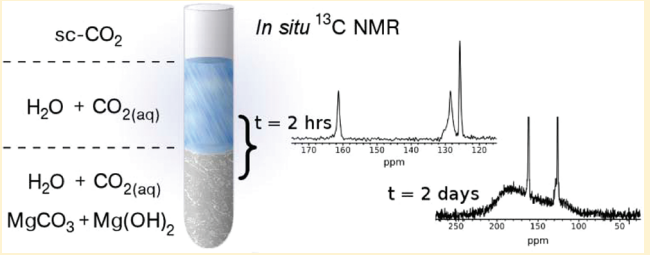

I. INTRODUCTION

Due to rising carbon levels in the atmosphere, there is much interest in the chemical and physical implications of carbon sequestration, a process by which CO_2 generated as a byproduct of energy production (or other industrial processes, such as cement production) is captured and stored instead of being released into the atmosphere. While many different storage mechanisms have been and continue to be considered,[1−3] one of the most promising is geological sequestration, where the captured CO_2 is pressurized and pumped deep underground into geological formations. It is so promising because of the massive containment volume that this method offers (~100 trillion tons of CO_2 globally, assuming complete mineralization).[4,5]

CO_2 geological storage is accomplished through one or more entrapment mechanisms:[5,6] stratigraphic (physically trapped CO_2), solubility (CO_2 dissolved in the geological brine), hydrodynamic (dissolved CO_2 trapped due to slow flow of geological brine), residual (CO_2 trapped in pore spaces by capillary pressure), and chemical (CO_2 reacts with a divalent metal, such as Mg^{2+}, Ca^{2+}, or Fe^{2+}, to form highly stable solid carbonates). Chemical trapping, or mineralization, is widely considered to be the most secure form of geological entrapment since the CO_2 has been converted into an immobile, more chemically stable state and is not merely physically trapped.[5−7] Here we focus on mineralization reactions of CO_2.

Solid carbonates are formed when a divalent cation reacts with the anionic carbonate species (CO_3^{2-}).[2,4−6] Successful formation of the carbonates therefore depends on the concentration and availability of the metal cation *and* the carbonate anion in the solution, in addition to favorable conditions for precipitation and crystallization. In geological CO_2 sequestration, sites are selected that contain significant quantities of these cations in the brine solution and in the minerals present, which are released when the pH of the brine dissolves the mineral into its constituent ionic species.[2,4−6] The carbonate anion comes from the reaction of CO_2 with water.

Many studies[6,8−10] have focused on the carbonation of the magnesium-containing mineral olivine, $Mg_xFe_{2-x}SiO_4$, because it has the highest magnesium fraction among rock-forming minerals present in candidate sequestration sites. Olivine is also the singly most abundant mineral in the earth's upper mantle and has the fastest carbonation rate of the naturally occurring minerals.[11] Olivine that contains no iron is called forsterite, Mg_2SiO_4, and is the primary constituent in naturally occurring olivine, $Mg_{1.8}Fe_{0.2}SiO_4$.

Special Issue: Carbon Sequestration

Received: April 1, 2012
Revised: May 26, 2012
Accepted: June 1, 2012

   dx.doi.org/10.1021/es301287n | *Environ. Sci. Technol.* XXXX, XXX, XXX−XXX

As forsterite contains two units of MgO and one of SiO_2 (quartz), reacting carbonation systems of Mg_2SiO_4 are often addressed in terms of a simplified $MgO-CO_2-H_2O$ phase diagram,[12] since MgO is the constituent of interest. Every chemical intermediate in that ternary system corresponds to different stoichiometric amounts of the three constituents MgO, CO_2, and H_2O, with the exception of SiO_2. SiO_2 dissolves and reprecipitates during the reaction, and is thus not a chemical participant in the reaction as long as there is an abundance of water.[5,10,13,14] We have selected the magnesium-containing species brucite, $Mg(OH)_2$, as a model system where carbonate formation can be studied in a straightforward manner. Though brucite is not present geologically in quantities significant enough for use in sequestration, studies of such a mineral as a model system allows the carbonation of magnesium to be elucidated, without complications from the parallel process of dissolution and precipitation of SiO_2. In addition to sequestration applications, minerals such as brucite (or periclase, MgO) also have potential applications as CO_2 scrubbers in an industrial setting.[15]

The mineralization processes in sequestration reactions are kinetically hindered and depend on the rates of several sequential reaction steps.[6] These steps are summarized in the following four chemical equations:

$$CO_{2(g)} \leftrightarrow CO_2(aq) \quad (1)$$

$$CO_{2(aq)} + H_2O \leftrightarrow HCO_3^- + H^+ \leftrightarrow CO_3^{2-} + 2H^+ \quad (2)$$

$$Mg(OH)_2 + 2H^+ \leftrightarrow Mg^{2+} + 2H_2O \quad (3)$$

$$Mg^{2+} + CO_3^{2-} \rightarrow MgCO_3 \quad (4)$$

Equation 1 describes the dissolution of CO_2 into the geological brine. Equation 2 describes the two-step reaction of CO_2 with water to form bicarbonate and carbonate ions. Equation 3 describes the dissolution of a nearby mineral, in this case brucite [$Mg(OH)_2$], and finally Equation 4 describes the formation of $MgCO_3$ product by precipitation.

Here we report on the development of a new static, in situ, noninvasive ^{13}C NMR spectroscopy under high pressure and temperature conditions that possesses the ability to monitor the chemical evolution of supercritical (sc) CO_2 in unmixed, sequestration-like conditions. While others have completed related high-pressure ^{13}C NMR experiments,[16,17] our method distinguishes itself by both monitoring mineralization in an unmixed, nonspinning system and using a solid mineral as a reactant. A static, unmixed system is significant in that this technique enables the observation of spatially dependent reaction products in the heterogeneous reaction mixture due to reactant gradients that are more reflective of true sequestration conditions.

II. EXPERIMENTAL SECTION

Ninety-nine percent ^{13}C-labeled $^{13}CO_2$ gas from Sigma Aldrich was used in the reactions reported here. Brucite (0.761 g), $Mg(OH)_2$, with purity exceeding 98% was used as-received from Alpha Aesar and mixed with 2.7 mL of distilled water to form a heterogeneous mixture with an excess of water (molar ratio of mineral/water was 8.7%). The less than 2% impurities in the brucite are soluble salts left over from the manufacturing process.

For NMR experiments, the T_1 spin−lattice relaxation time of ^{13}C of CO_2 (aq) in this system is ∼7 s at 80 °C and 88 bar and ∼35 s at room temperature (22 °C). The relaxation time of ^{13}C of HCO_3^- (aq) is ∼1 s, and the magnesium carbonate products' are ∼7 s at room temperature, shorter for both species at higher temperatures. Because of these long spin−lattice relaxation times, $\pi/4$ excitation pulses were used to enhance signal-to-noise ratios at shorter recycle delays.

Static in Situ ^{13}C NMR. A typical $\pi/2$ pulse length is approximately 30 μs for this probe. NMR experiments were conducted using Bloch decay pulse sequences with $\pi/4$ pulses and recycle delays of 10 s at an observe frequency of 89.07 MHz for ^{13}C, without ^1H decoupling. The high-pressure sample tube (with loaded sample, described below) was placed under modest vacuum (0.1 bar) before connecting to the $^{13}CO_2$ source in order to remove most of the O_2 and N_2 gases from the apparatus without dehydrating the sample. Chemical shift referencing was completed by using the highly stable $^{13}CO_2$ (aq) peak at 126.0 ppm.[16,18,19] It was found that the CO_2 peak's chemical shift does not change within experimental error at the reaction conditions considered in this paper, and therefore could serve as an internal reference.

Raman Spectroscopy. Raman was performed both "in situ" on the depressurized, but otherwise untouched, high-pressure sample tube, as well as ex situ on powders collected from the tube. The in situ Raman was performed by focusing the laser through the walls of the glass tube on the material inside. The glass produced small background fluorescence but did not inhibit observation of the reaction products. This method enabled spatial observation without disturbing the product morphology. Both Raman experiments were performed using a HoloLab Series 5000 Laser Raman Microprobe (Kaiser Optical). The microprobe delivered a 532-nm laser beam from a frequency-doubled Nd:YAG laser through a 20× (except where noted) long-working-distance objective with a 0.4 numerical aperture. This configuration delivered a maximum of 11 mW of laser power onto the sample; each spectrum had a resolution of about 3 cm^{-1} and was recorded from 100 to 4000 cm^{-1} with a reproducibility of 0.1 cm^{-1}. The sampled regions were about 5 μm in diameter with a penetration depth of a similar magnitude due to the highly scattering nature of the product crystals. Multiple spectra were obtained from the sample, even though not all are shown, to support conclusions and ensure that the microprobe was providing spectra indicative of the entire sample.

Powder X-ray Diffraction (pXRD). pXRD analysis was performed on a well-ground and mixed portion of the product sample to ensure that the pXRD results were a net average of the products made. The pXRD spectrum was obtained using a Rigaku Geigerflex D-MAX/A diffractometer with Cu−Kα radiation at 35 kV and 35 mA. The instrument was calibrated using the silicon (111) reflection at 28.443 degrees (2θ). The pXRD pattern was obtained at room temperature from 10 to 65 degrees (2θ). Analysis of spectra, including background removal, was completed using Jade Plus software. The PDF-4 and American Mineralogist powder diffraction databases were used for the matching of different reference patterns (amcsd 0009586, PDF 01-075-8824, 00-023-1218, 00-007-0239).

Ex Situ $^{13}C\{^1H\}$ MAS NMR. ^1H-decoupled ^{13}C MAS NMR experiments were performed using a 4-mm Varian HXMAS NMR probe on solids collected from the high-pressure sample tube after completion of all reactions, with a ^{13}C observe

dx.doi.org/10.1021/es301287n | Environ. Sci. Technol. XXXX, XXX, XXX−XXX

frequency of 74.02 MHz and ^{1}H decoupling frequency of 294.38 MHz, at a MAS rotational frequency of 5 kHz. Typical experimental parameters include a $\pi/4$ pulse that was 1.5 μs with a recycle delay of 5 s, recording 256 scans. Samples were externally referenced to adamantane's −CH carbon at 28.680 ppm, which is a secondary reference based on ^{13}C of tetramethylsilane at 0 ppm.

III. RESULTS AND DISCUSSION

A. In Situ ^{13}C NMR. The reactions were carried out in a home-built high-pressure and -temperature solid-state NMR probe in which all of the static solid-state ^{13}C NMR spectra were obtained. Thus, the NMR was performed on the reacting system (i.e., in situ NMR, as opposed to ex situ NMR after the reaction has been quenched and subsequently sampled). This combination NMR probe plus reactor enabled monitoring of the uptake of CO_2 and the precipitation of various carbonate products during the reaction.

The home-built solid-state NMR probe is able to achieve reaction conditions (i.e., temperatures up to 250 °C, pressures up to 300 bar) similar to those found in geological sequestration environments[6,20,21] by using a zirconia high-pressure sample tube (dimensions: 15.24 mm outer diameter, 10.03 mm inner diameter, 73.66 mm length, and closed at one end) contained within a well-insulated zone heated by flowing temperature-regulated air. A glass liner was placed inside the high-pressure vessel to allow easy removal of reaction products and to prevent carbonate from crystallizing on the zirconia tube itself (which proved difficult to remove). The radio frequency NMR coil is situated outside the high-pressure zirconia vessel and is of an Alderman−Grant design.[22] A $^{13}CO_2$ source was cryogenically pressurized for both reactions studied here and was delivered into the high-pressure vessel in the liquid state. Supercritical (sc) conditions were achieved by warming the heating zone around the vessel. Figure 1 is a schematic of the reaction setup in the high-pressure tube, with sc-CO_2 in the headspace over water-soaked mineral powder. The coil was placed around the high-pressure vessel in such a way that the vessel could be moved up and down, allowing ^{13}C NMR spectra to be collected specifically on the solution above the powder, within the powder, or centered at the interface between the two.

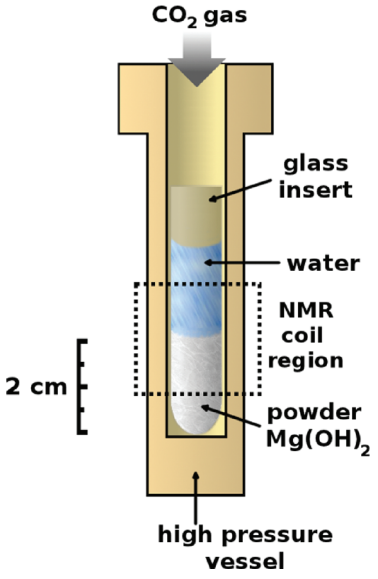

Figure 1. Cross-section of the zirconia high-pressure vessel for in situ NMR.

The heating zone's temperature (and subsequent reaction temperature) was measured by a type E thermocouple placed next to the high-pressure vessel, in the heated zone. The internal temperature of the high-pressure vessel was calibrated from a previous experiment during which an additional type E thermocouple was placed at difference positions in a water solution within the length of the high-pressure vessel. The entire NMR coil region as well as areas directly above and below within the high-pressure vessel assumed the same temperature as the heated zone around it with a small lag time during warming and cooling events. This test ensured that the probe did not induce a temperature gradient across the sample during high-pressure and -temperature experiments.

Solid Carbonate Formation. Conversion of CO_2 into magnesium carbonates can be monitored by NMR as shown in Figures 2 and 3. Solid brucite powder was added to the distilled water to create a heterogeneous mixture. Brucite was chosen to demonstrate the feasibility of this method because it quickly reacts with CO_2 when exposed to sequestration-like conditions.[7,15]

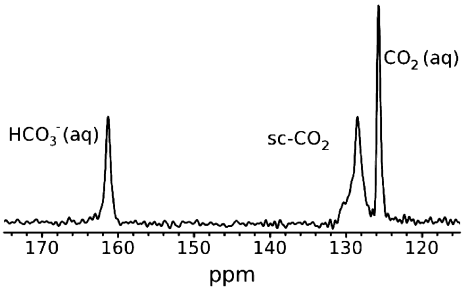

Figure 2. ^{13}C static NMR of reaction mixture of CO_2 and a slurry of water and brucite, $Mg(OH)_2$, recorded 2 h into the reaction before any mineralization had been detected. Conditions were 80 °C and 91.8 bar. The aqueous CO_2 and supercritical CO_2 have slightly different resonance frequencies because of magnetic susceptibility effects.

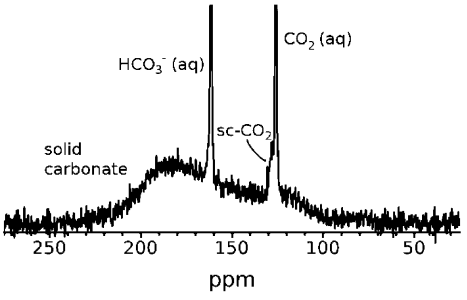

Figure 3. ^{13}C static NMR of CO_2 and a slurry of water and brucite, recorded 58 h into the reaction at 80 °C and 88.5 bar. The broad feature underlying the sharp resonances is the powder pattern indicative of a solid carbonate species. The HCO_3^- and CO_2 peaks are truncated (off-scale) so that the powder pattern is clearly evident.

The brucite and water mixture was allowed to sit overnight so that the solid phase settled, making two distinct layers: liquid on top and water-saturated brucite powder on the bottom. The mixture was heated to 80 °C upon introduction of $^{13}CO_2$ and pressurized to 93 bar, which slowly dropped to 88 bar as some of the CO_2 dissolved into the water and began to react.

dx.doi.org/10.1021/es301287n | Environ. Sci. Technol. XXXX, XXX, XXX−XXX

Even though brucite is only sparingly soluble, its presence in the solution makes the solution basic, raising the pH and thereby shifting the $CO_2 + H_2O \leftrightarrow HCO_3^- + H^+$ equilibrium (eq 2) considerably more to the right, increasing the relative HCO_3^- concentration. Two hours into the reaction, as shown in Figure 2, both aqueous and supercritical CO_2 are observed (see Figure S1 for justification of peak assignments), in addition to aqueous HCO_3^-. Since the ^{13}C NMR peak areas are quantitative indicators of the amount of each species, this early stage in the reaction shows that the HCO_3^- concentration is close to that of aqueous CO_2.

After more than two days of reaction (58 h) at elevated temperature and pressure, a ^{13}C solid-state carbonate powder pattern emerged (Figure 3), indicating solid carbonate precipitation. The solid-state signals are broad because of the absence of reorientational motions, which narrow the resonances in fluid phases. With the absence of motion, the chemical shift is dependent upon the orientation of the ^{13}C nucleus' environment relative to the magnetic field (chemical shift anisotropy) and generates a "powder pattern" based on the fractional distribution of nuclei in each molecular orientation. The HCO_3^- and CO_2 (aq) peaks are off-scale in order to depict the shape and height of the carbonate powder pattern, which resembles that of well-studied calcium carbonate[23,24] and is similar to the measured magnesium carbonate pattern but with some important differences that indicate that there are other carbonate phases contributing to the powder pattern (see Figure S2).

At 60 h of reaction, the temperature was lowered by blowing room-temperature air into the heating zone around the high-pressure vessel. After cooling to room temperature, the high-pressure vessel was depressurized slowly (over a 60-min period), to prevent $^{13}CO_2$ gas from bubbling out of the solution and forming a foam. The glass insert was then removed from the reaction vessel and capped so that spatially resolved Raman experiments could be run on the sample immediately. After the Raman experiments, the aqueous solution was pulled off of the solid sample using a pipette, and the remaining solid product was placed in a vacuum chamber overnight at room temperature to dry. A small amount of sample was removed from the dried product at both the top of the sample and deeper into the sample, was crushed and finely ground for proper pXRD analysis using an agate mortar and pestle, and ex situ analysis was performed.

Postreaction analysis of solid carbonate phases was accomplished through three complementary techniques: Raman spectroscopy, powder X-ray diffraction (pXRD), and ^{13}C MAS NMR, all of which provided additional information on the different carbonate phases that were formed during the reaction.

B. "In Situ" and ex Situ Raman. Figure 4 displays the in situ Raman spectra obtained by focusing the laser through the glass sample tube that was still wet and contained both solution and solid from the reaction. The tube and its contents had been depressurized only minutes before these spectra were obtained and had not been subjected to any other treatment. While the glass tube produced very little fluorescence, it was enough to prevent quantitative comparison between the different spectra. Instead, a relative comparison of the fraction of each peak area in each spectrum can be compared from one spectrum to another to see the spatial distribution of the products. It is important to note that all peaks observed in the Raman spectrum were analyzed and consistent with previously

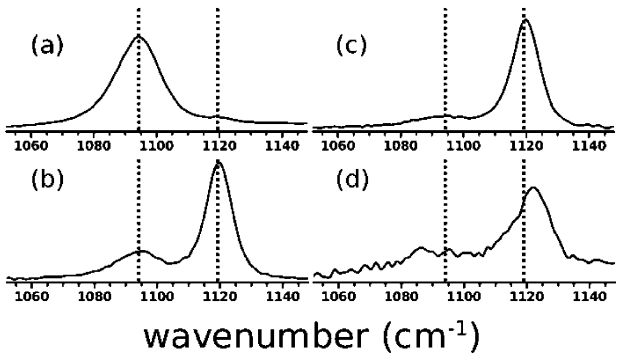

Figure 4. Raman spectra of the reaction products in the range of the characteristic CO_3^{2-} symmetric stretches, each taken at different points along the length of the sample tube: (a) at the solution/solid interface (0.0 cm), (b) 0.25 cm below the interface, (c) 0.5 cm, and (d) 0.6 cm. Spectra (b)−(d) were acquired at 5× magnification and thus have different arbitrary intensity scales than (a). In addition, the *y*-axis in spectrum (d) has been expanded so as to better see the peaks. The lines at 1094 and 1119 cm^{-1} are guides to the eye for the locations of the magnesite and hydromagnesite/dypingite peaks, respectively.

reported assignments, and only the symmetric CO_3^{2-} symmetric stretching frequencies are shown here. These stretching frequencies are considered to be very good indicators of the identities of some carbonate minerals[25,26] and are unaffected by the change in carbon isotope (to 99% ^{13}C) because the carbon atom remains at rest in the symmetric stretching mode.

The peak at 1094 cm^{-1} is indicative of magnesite ($MgCO_3$),[25] while the peak at 1119 cm^{-1} is in the region of other hydroxy-hydrated metastable carbonate species, namely hydromagnesite and dypingite[27,28] [$4MgCO_3{\cdot}Mg(OH)_2{\cdot}4H_2O$ and $4MgCO_3{\cdot}Mg(OH)_2{\cdot}5H_2O$, respectively].[25,26,29] While both hydromagnesite and dypingite are difficult to differentiate using any method besides pXRD, literature suggests that dypingite has its symmetric stretch in the 1120−1124 cm^{-1} region,[29] slightly different from hydromagnesite's well-defined 1119 cm^{-1} stretch.[25] The trend in Figure 4 therefore suggests that the reaction is complete at the solution/solid interface end-state product (dominated by $MgCO_3$), and becomes less complete (more hydroxy-hydrated carbonate products) as one observes locations further down the length of the tube, with the hydromagnesite species being the dominant species at shallower regions, gradually transitioning to dypingite at the lowest, deepest regions. No carbonate signals could be observed at depths greater than 0.7 cm into the sample, and no Raman peaks for $^{13}CO_2$ were observed.

Previous research[7,12,15,26,30,31] summarizes the extensive experimental and computational results from the MgO−CO_2−H_2O system. It is clear from these results that temperature and partial pressure of CO_2 are both of primary importance in directing which mineral forms preferentially. The products are not always the most thermodynamically stable, as there are kinetic inhibitions in these reactions, which has been discussed in great detail by others.[7,12,26,31,32] At room temperature and ambient to moderate CO_2 pressures, the basic carbonate mineral nesquehonite [$Mg(OH)(HCO_3){\cdot}2H_2O$] forms.[7] At higher temperatures, above approximately 40 °C, hydromagnesite becomes the primary carbonate product.[26] Anhydrous magnesite forms only at even higher temperatures (>60−100 °C),[12,33,34] and only if higher CO_2 pressures are present.[6,26,32]

dx.doi.org/10.1021/es301287n | Environ. Sci. Technol. XXXX, XXX, XXX−XXX

Dypingite, a lesser-known mineral, is very similar to hydromagnesite in composition but is less stable and can be considered an intermediate hydrate phase between nesquehonite and hydromagnesite.[28,35] Its molecular formula has been reported with different numbers of waters throughout literature, but is generally thought of as a more-hydrated version of hydromagnesite. Its observation ex situ may also be a result of small amounts of mineralization during the cooling, depressurization, and drying process, even though great effort was made to make this process as fast as possible. Generally, dypingite is regarded to form at slightly higher temperatures than that of nesquehonite,[36] and some evidence exists that it is more likely to form under more basic conditions.[37] In addition, dypingite can be observed in nature, like magnesite and hydromagnesite, but is generally only found in cooler climates[27−29,38] as warm temperatures will speed its conversion to hydromagnesite.

At the pressure and temperature conditions reported here (80 °C and 88 bar), any or all magnesite, hydromagnesite, and dypingite could exist.

After drying the sample and removing it from the tube, a small sample from the middle portion of the tube was removed and examined via ex situ Raman (see Figure S3). Well-defined coexistent peaks indicate the presence of both magnesite and hydromagnesite/dypingite, and no Raman peaks for $^{13}CO_2$ were seen in the analysis. The increased breadth of the magnesite peak (as compared to our magnesite standard and the hydromagnesite/dypingite peak) in both in situ and ex situ experiments indicates that other hydrated phases of magnesium carbonate might be present, coexisting with the magnesite, and/or that the magnesite phase is composed of extremely small crystallites.

C. Ex situ X-ray Powder Diffraction. Figure 5 shows the diffraction pattern and analysis. The pattern confirms the coexistence of dypingite, hydromagnesite, and magnesite, with little or no remaining brucite. These results are consistent with our findings from Raman spectroscopy.

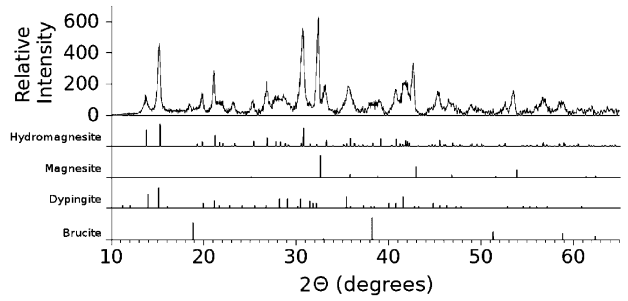

Figure 5. X-ray diffraction pattern from the reaction product. The magnesite peaks are shifted by ∼1° from the reference magnesite spectrum, suggesting that the unit cell is expanded.

As XRD is a time- and space-averaged measurement,[39] the smaller 2θ values (∼1° left-shifted) indicate that some of the $MgCO_3$ unit cells have expanded. The unit cell expansion is likely due to incomplete removal of water during the hydromagnesite-to-magnesite transition[26] leading to partial hydration. It is also important to note that nesquehonite $[Mg(HCO_3)(OH)\cdot 2H_2O]$ was not observed in the reaction products, probably because the reaction temperature was too high.[35]

D. Ex situ $^{13}C\{^1H\}$ MAS. Proton-decoupled ^{13}C solid-state magic-angle spinning (MAS) NMR on the powder collected from the top portion of the sample from the high-pressure sample tube shows multiple solid carbonate species present in the reaction product (Figure 6). A resonance at 169.2 ppm confirmed the existence of magnesite, $MgCO_3$.[40] Two other peaks, at 164.7 and 162.6 ppm, are suggestive of the coexistence of hydromagnesite and dypingite[27,28] in agreement with the pXRD data. Recent research proposes assignments for hydromagnesite and dypingite, each with two resonances that are very close to one another.[14] Hydromagnesite has been assigned to two peaks of equal area at 166.4 and 164.1 ppm (further substantiated by its single-crystal XRD structure showing two inequivalent carbons[41]), while dypingite has been assigned to two peaks of unequal area at 165.7 and 163.4 ppm.[14] The differences between our reported chemical shift values for these species and the recent research can be explained by the error between the two different chemical shift referencing techniques used in the two studies. As our reported peaks at 164.7 and 162.6 ppm (Figure 6) have unequal areas, this implies a possible mixture of hydromagnesite and dypingite.

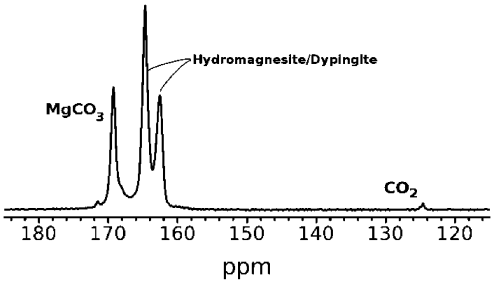

Figure 6. Ex situ ^{13}C MAS NMR spectrum (with ^1H decoupling) of the upper reaction product. The CO_2 peak is residual CO_2, most likely physically trapped in the solid phase.

There are three other resonances of note in Figure 6: a peak at 124.7 ppm, which is likely $^{13}CO_2$ trapped in the precipitated crystal product; an unidentified small peak at 171.5; and an unidentified small shoulder on the magnesite peak at ∼168 ppm. The two unidentified peaks could be other morphologically distinct phases of $MgCO_3$, such as singly hydrated $MgCO_3$. It is known that singly hydrated calcite $(CaCO_3\cdot H_2O)$ has a slightly higher-frequency ^{13}C chemical shift relative to its anhydrous counterpart $(CaCO_3)$, changing from 168.21 to 171.10 ppm,[42] supporting this preliminary interpretation. While the areas of the $MgCO_3$ peaks (171.5, 169.1, and 168 ppm) cannot be precisely compared due to potential differences in their T_1 relaxation times, the spectrum suggests that there is vastly more $MgCO_3$ as compared to its morphologically distinct counterparts at 171.5 and 168 ppm. Further, ^{13}C MAS NMR demonstrates that $MgCO_3$ (magnesite) and hydroxy-hydrated forms (like dypingite and hydromagnesite) are the major reaction products.

Figure 7 is a spectrum obtained from a lower portion of the sample, further confirming the spatial dependence of the products that were formed. Recorded in the same manner as the spectrum in Figure 6, it is evident that there are no $MgCO_3$ phases, with only the two peaks characteristic of hydromagnesite and dypingite present. Their increased breadth indicates a less-crystalline phase, and the reduced signal-to-noise ratio of the spectrum indicates less total carbonate product. Furthermore, no residual CO_2 was detected.

dx.doi.org/10.1021/es301287n | Environ. Sci. Technol. XXXX, XXX, XXX−XXX

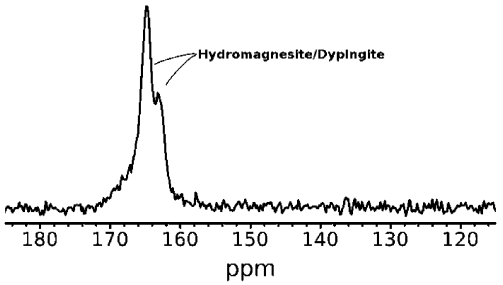

Figure 7. Ex situ ^{13}C MAS NMR spectrum (with ^{1}H decoupling) of the lower reaction product. There are two prominent peaks located at 162.8 and 164.8 ppm.

Precise determination of the relative amounts of the different solid-state products was not possible in these experiments, although the chemical identities found using MAS NMR confirm results from Raman and pXRD experiments. Raman (Figure 4) and ^{13}C MAS NMR results (Figures 6 and 7) suggest, however, that the relative amount of each possible product varies by depth into the sample. Magnesite exists only in the layers closest to the solution/solid interface, with increasing amounts of coexisting dypingite and hydromagnesite deeper into the sample. The pXRD pattern (Figure 5) fortifies our ^{13}C NMR and Raman results by further confirming the existence of these phases in our sample.

The spatial dependence of the products demonstrates the importance of a static reacting system when studying sequestration reactions. This experiment has the advantages of incorporating both the chemistry and physics of sequestration reactions. We surmise that the physical barrier that a solid imposes on the pivotal reactant CO_2 (aq) restricts its diffusion and therefore makes a spatial dependence of products based on the local pH and carbon concentration gradient.

While the results presented in this paper demonstrate the new ability to monitor sequestration reactions in situ, subsequent work will also expand the reactions to additional mineral and rock systems, as well as different pressures and systems, as well as different pressures and temperatures. We also intend to further investigate the cause of the spatial dependency of the products in these reacting systems.

■ ASSOCIATED CONTENT

Supporting Information

Additional spectra and simulations. This information is available free of charge via the Internet at http://pubs.acs.org/

■ AUTHOR INFORMATION

Corresponding Author

*E-mail: hayes@wustl.edu; tel.: (314) 935-4624; fax: (314) 935-4481 (S.E.H.); e-mail: msc@wustl.edu; tel.: (314) 935-6418; fax: (314) 935-6219 (M.S.C.).

Notes

The authors declare no competing financial interest.

■ ACKNOWLEDGMENTS

This research was supported by a grant from the Washington University Consortium for Clean Coal Utilization (CCCU). We thank Prof. Jill Pasteris (WU, Earth & Planetary Sciences) for assistance with Raman spectra, and Ms. Katie Wentz (WU, Chemistry) for MAS NMR assistance.

■ REFERENCES

(1) House, K. Z. Permanent carbon dioxide storage in deep-sea sediments. *Proc. Natl. Acad. Sci.* **2006**, *103*, 12291−12295.

(2) Lackner, K. S. Carbonate chemistry for sequestering fossil carbon. *Ann. Rev. Energy Environ.* **2002**, *27*, 193−232.

(3) Drange, H.; Alendal, G.; Johannessen, O. M. Ocean release of fossil fuel CO_2: A case study. *Geophys. Res. Lett.* **2001**, *28*, 2637.

(4) Kelemen, P. B.; Matter, J. From the Cover: In situ carbonation of peridotite for CO_2 storage. *Proc. Natl. Acad. Sci.* **2008**, *105*, 17295−17300.

(5) Matter, J. M.; Kelemen, P. B. Permanent storage of carbon dioxide in geological reservoirs by mineral carbonation. *Nat. Geosci.* **2009**, *2*, 837−841.

(6) Giammar, D. E.; Bruant, R. G.; Peters, C. A.; Bruant, R., Jr. Forsterite dissolution and magnesite precipitation at conditions relevant for deep saline aquifer storage and sequestration of carbon dioxide. *Chem. Geol.* **2005**, *217*, 257−276.

(7) Xiong, Y.; Lord, A. S. Experimental investigations of the reaction path in the $MgO−CO_2−H_2O$ system in solutions with various ionic strengths, and their applications to nuclear waste isolation. *Appl. Geochem.* **2008**, *23*, 1634−1659.

(8) Hanchen, M.; Prigiobbe, V.; Storti, G.; Seward, T.; Mazzotti, M. Dissolution kinetics of fosteritic olivine at 90−150°C including effects of the presence of CO_2. *Geochim. Cosmochim. Acta* **2006**, *70*, 4403−4416.

(9) Loring, J. S.; Thompson, C. J.; Wang, Z.; Joly, A. G.; Sklarew, D. S.; Schaef, H. T.; Ilton, E. S.; Rosso, K. M.; Felmy, A. R. In Situ Infrared Spectroscopic Study of Forsterite Carbonation in Wet Supercritical CO_2. *Environ. Sci. Technol.* **2011**, *45*, 6204−10.

(10) Kwak, J. H.; Hu, J. Z.; Hoyt, D. W.; Sears, J. A.; Wang, C.; Rosso, K. M.; Felmy, A. R. Metal Carbonation of Forsterite in Supercritical CO_2 and H_2O Using Solid State ^{29}Si, ^{13}C NMR Spectroscopy. *J. Phys. Chem. C* **2010**, *114*, 4126−4134.

(11) Kelemen, P. B.; Matter, J. M.; Streit, L.; Rudge, J. F.; Curry, W. B.; Blusztajn, J. S.; Streit, E. E. Rates and Mechanisms of Mineral Carbonation in Peridotite: Natural Processes and Recipes for Enhanced, in situ CO_2 Capture and Storage. *Ann. Rev. Earth Planet. Sci.* **2010**, *39*, 545−576.

(12) Bénézeth, P.; Saldi, G. D.; Dandurand, J.-L.; Schott, J. Experimental determination of the solubility product of magnesite at 50 to 200 °C. *Chem. Geol.* **2011**, *286*, 21−31.

(13) Lackner, K. S.; Wendt, C. H.; Butt, D. P.; Joyce, E. L.; Sharp, D. H. Carbon dioxide disposal in carbonate minerals. *Energy* **1995**, *20*, 1153−1170.

(14) Kwak, J. H.; Hu, J. Z.; Turcu, R. V. F. F.; Rosso, K. M.; Ilton, E. S.; Wang, C.; Sears, J. A.; Engelhard, M. H.; Felmy, A. R.; Hoyt, D. W. The role of H_2O in the carbonation of forsterite in supercritical CO_2. *Int. J. Greenhouse Gas Control* **2011**, *5*, 1081−1092.

(15) Zhao, L.; Sang, L.; Chen, J.; Ji, J.; Teng, H. H. Aqueous carbonation of natural brucite: relevance to CO_2 sequestration. *Environ. Sci. Technol.* **2010**, *44*, 406−11.

(16) Hoyt, D. W.; Turcu, R. V. F.; Sears, J. A.; Rosso, K. M.; Burton, D.; Felmy, A. R.; Hu, J. Z.; Burton, S. D. High-Pressure Magic Angle Spinning Nuclear Magnetic Resonance. *J. Magn. Reson.* **2011**, *212* (2), 378−385.

(17) Diefenbacher, J.; Piwowarczyk, J.; Marzke, R. F. Note: Solution NMR probe for the study of CO_2 sequestration at elevated pressure and temperature. *Rev. Sci. Instrum.* **2011**, *82*, 076107.

(18) Abbott, T. M.; Buchanan, G. W.; Kruus, P.; Lee, K. C. ^{13}C nuclear magnetic resonance and Raman investigations of aqueous carbon dioxide systems. *Can. J. Chem.* **1982**, *60*, 1000−1006.

(19) Jakobsen, J. P.; Krane, J.; Svendsen, H. F. Liquid-Phase Composition Determination in $CO_2−H_2O−$Alkanolamine Systems: An NMR Study. *Ind. Eng. Chem. Res.* **2005**, *44*, 9894−9903.

(20) Rosenbauer, R. J.; Koksalan, T.; Palandri, J. L. Experimental investigation of $CO_2−$brine−rock interactions at elevated temperature and pressure: Implications for CO_2 sequestration in deep-saline aquifers. *Fuel Process. Technol.* **2005**, *86*, 1581−1597.

(21) Spycher, N.; Pruess, K.; Ennis-King, J. CO_2-H_2O mixtures in the geological sequestration of CO_2. I. Assessment and calculation of mutual solubilities from 12 to 100°C and up to 600 bar. *Geochim. Cosmochim. Acta* **2003**, *67*, 3015−3031.
(22) Alderman, D. W.; Grant, D. M. An efficient decoupler coil design which reduces heating in conductive samples in superconducting spectrometers. *J. Magn. Reson. (1969-1992)* **1979**, *36*, 447−451.
(23) Lauterbur, P. Anisotropy of the C^{13} chemical shift in calcite. *Phys. Rev. Lett.* **1958**, *1*, 343−344.
(24) Pines, A. ^{13}C Chemical Shielding Anisotropy in Solids. CS_2 and $CaCO_3$. *J. Chem. Phys.* **1971**, *54*, 5438.
(25) Edwards, H. G. M.; Villar, S. E. J.; Jehlicka, J.; Munshi, T. FT-Raman spectroscopic study of calcium-rich and magnesium-rich carbonate minerals. *Spectrochim, Acta, Part A* **2005**, *61*, 2273−80.
(26) Hanchen, M.; Prigiobbe, V.; Baciocchi, R.; Mazzotti, M. Precipitation in the Mg-carbonate system—effects of temperature and CO_2 pressure. *Chem. Eng. Sci.* **2008**, *63*, 1012−1028.
(27) Raade, G. Dypingite, a new hydrous basic carbonate of magnesium, from Norway. *Am. Mineral.* **1970**, *55*, 1457−1465.
(28) Canterford, J. H. Some Observations on the Properties of Dypingite, $Mg_5(CO_3)_4(OH)_2{\cdot}5H_2O$, and Related Minerals. *Mineral. Mag.* **1984**, *48*, 437−442.
(29) Frost, R. L.; Bahfenne, S.; Graham, J. Raman spectroscopic study of the magnesium-carbonate minerals-artinite and dypingite. *J. Raman Spectrosc.* **2009**, *40*, 855−860.
(30) Case, D. H.; Wang, F.; Giammar, D. E. Precipitation of Magnesium Carbonates as a Function of Temperature, Solution Composition, and Presence of a Silicate Mineral Substrate. *Environ. Eng. Sci.* **2011**, *28*, 881−889.
(31) Königsberger, E.; Königsberger, L.-C.; Gamsjäger, H. Low-temperature thermodynamic model for the system Na_2CO_3−$MgCO_3$−$CaCO_3$−H_2O. *Geochim. Cosmochim. Acta* **1999**, *63*, 3105−3119.
(32) Sayles, F. L.; Fyfe, W. S. The crystallization of magnesite from aqueous solution. *Geochim. Cosmochim. Acta* **1973**, *37*, 87−99.
(33) Sandengen, K.; Jøsang, L. O.; Kaasa, B. Simple Method for Synthesis of Magnesite ($MgCO_3$). *Ind. Eng. Chem. Res.* **2008**, *47*, 1002−1004.
(34) Xing, Z.; Hao, Q.; Ju, Z.; Xu, L.; Qian, Y. Synthesis of $MgCO_3$ microcrystals at 160°C starting from various magnesium sources. *Mater. Lett.* **2010**, *64*, 1401−1403.
(35) Davies, P. J.; Bubela, B. The transformation of nesquehonite into hydromagnesite. *Chem. Geol.* **1973**, *12*, 289−300.
(36) Pronost, J.; Beaudoin, G.; Tremblay, J.; Larachi, F.; Duchesne, J.; Hébert, R.; Constantin, M. Carbon sequestration kinetic and storage capacity of ultramafic mining waste. *Environ. Sci. Technol.* **2011**, *45*, 9413−20.
(37) Wilson, S. a; Barker, S. L. L.; Dipple, G. M.; Atudorei, V. Isotopic disequilibrium during uptake of atmospheric CO_2 into mine process waters: Implications for CO_2 sequestration. *Environ. Sci. Technol.* **2010**, *44*, 9522−9.
(38) Jujin Suzuki, M. I. A new magnesium carbonate hydrate mineral, $Mg_5(CO_3)_4(OH)_2{\cdot}8H_2O$, from Yoshikawa, Aichi prefecture, Japan. *J. Jpn. Assoc. Mineral., Petrol. Econ. Geol.* **1973**, 353−361.
(39) Halasz, I. Single-Crystal-to-Single-Crystal Reactivity: Gray, Rather than Black or White. *Cryst. Growth Des.* **2010**, *10*, 2817−2823.
(40) Papenguth, H. W. W.; Kirkpatrick, R. J. J.; Montez, B.; Sandberg, P. A. A. ^{13}C MAS NMR spectroscopy of inorganic and biogenic carbonates. *Am. Mineral.* **1989**, *74*, 1152−1158.
(41) Akao, M.; Marumo, F.; Iwai, S. The crystal structure of hydromagnesite. *Acta Crystallogr., Sect. B Struct. Crystallogr. Cryst. Chem.* **1974**, *30*, 2670−2672.
(42) Nebel, H.; Neumann, M.; Mayer, C.; Epple, M. On the structure of amorphous calcium carbonate--A detailed study by solid-state NMR spectroscopy. *Inorg. Chem.* **2008**, *47*, 7874−9.